Measuring *n* and *k* at the Microscale in Single Crystals of $CH_3NH_3PbBr_3$ Perovskite

*Sarah Brittman and Erik. C. Garnett**

Center for Nanophotonics, FOM Institute AMOLF, Science Park 104, Amsterdam 1098 XG, The Netherlands

AUTHOR INFORMATION

Corresponding Author

*Email: garnett@amolf.nl.

ABSTRACT

Lead-based, inorganic-organic hybrid perovskites have shown much promise in photovoltaics, and the ability to tune their band gap makes them attractive for tandem solar cells, photodetectors, light-emitting diodes, and lasers. A crucial first step toward understanding a material's behavior in such optoelectronic devices is determining its complex refractive index, $n+ik$; however, optically smooth films of hybrid perovskites are challenging to produce, and the optical properties of films of these materials have been shown to depend on the size of their crystallites. To address these challenges, this work reports quantitative reflectance and transmittance measurements performed on individual microcrystals of $CH_3NH_3PbBr_3$, with thicknesses ranging from 155 to 1907

nm. The single crystals are formed by spincoating a film of precursor solution and then stamping it with polydimethylsiloxane (PDMS) during crystallization. By measuring crystals of varying thickness, *n* and *k* values at each wavelength (405-1100 nm) have been determined, which agree with recently reported values extracted by ellipsometry on millimeter-sized single crystals. This approach can be applied to determine the optical constants of any material that presents challenges in producing smooth films over large areas, such as mixed-halide hybrid and inorganic perovskites, and to micro- or nanoplatelets.

In the last five years, lead-halide perovskite solar cells have leapt to the forefront of photovoltaic research[1] and are gaining ground in other optoelectronic fields such as light-emitting diodes (LEDs),[2-3] lasers,[4-5] and photodetectors.[6-8] Even miniaturization of these devices to the micro- and nanoscale is already underway.[9-13] Building on decades of hard-won insights from inorganic, organic, and dye-sensitized solar cells has enabled much of this rapid success. Perovskites combine some of the best attributes of these well-studied materials – the high absorption and solution-based processing of organics and dye-sensitized solar cells with the low recombination rates and excellent charge-transport properties more characteristic of inorganic semiconductor crystals.[14]

Researchers have found optoelectronic simulations of their materials and devices essential for rapid development, and abundant computing power and user-friendly simulation software have made these simulations more powerful and more accessible. By using such modeling, researchers can be confident in their analysis of experimental effects, understand nuances in their data, and predict improvements to the design of devices or geometries that lead to new phenomena. Simulations are only as accurate as

the data that go into them, however, so measuring fundamental properties of materials is essential. For optical simulations, this begins with the complex refractive index $n+ik$, or equivalently the complex dielectric constant $\varepsilon_1+i\varepsilon_2$.

Measurements of reflectance and transmittance[15-16] or ellipsometry[17] are the most common techniques for determining optical constants.[18-19] Both of these methods require fitting the data to an optical model, and the correspondence between the sample and the model determines the accuracy of the retrieved values. Surface roughness, variations in the thickness or composition of the film over the illuminated area, or surface coatings of oxides often complicate the fitting of experimental data.[17, 20-22] In the case of lead-halide hybrid perovskites, researchers have struggled to produce pinhole-free, optically smooth films on standard substrates such as glass or silicon. Ellipsometry accounting for a film's roughness has been used to determine optical constants for $CH_3NH_3PbI_3$ that agree well with absorption coefficients measured by photothermal deflection spectroscopy;[23-24] however, the grain size of perovskite films has been linked to their optical properties,[25] so it is essential to fully characterize the sample from which the optical constants are extracted. Also, as much as 70% of perovskite films can be disordered or amorphous material,[26] making the optical constants determined from them composite values. Such values are likely not applicable to films deposited using another method. In the case of $CH_3NH_3PbBr_3$, ellipsometry on macroscopic single crystals has recently yielded n and k values;[27] however, the slow solvothermal crystallization method used to produce such large crystals is quite different from the kinetically controlled process used to deposit the material commonly used in devices. A direct comparison of optical properties is therefore required.

To address these challenges, microscale reflectance[28-29] and transmittance measurements have been performed on flat and smooth single crystals of $CH_3NH_3PbBr_3$ produced by stamping with polydimethylsiloxane (PDMS). Regression analysis was applied to data from 22 crystals to extract the *n* and *k* values, and the resulting dispersion in the dielectric constants was fit with a Kramers-Kronig-consistent model.[30] $CH_3NH_3PbBr_3$ crystals exhibit a pronounced excitonic peak at their band edge, making this perovskite an intriguing material with which to study excitons at room temperature at visible wavelengths. As the first step in understanding the optical properties of this perovskite, these optical constants open up the possibility for the design and simulation of optoelectronic structures, as well as the fundamental study of exciton-polariton and exciton-plasmon coupling. This method can be applied widely to other materials for which microscale flakes of varying thicknesses are readily available, including the wide variety of mixed-halide hybrid and inorganic perovskites (Khoram, et al., manuscript in preparation). A similar micro-reflectance technique has also been used to determine optical constants of two-dimensional (2D) materials by invoking the Kramers-Kronig relations.[28]

Crystallization of the perovskite in contact with PDMS produced flat and smooth single crystals suitable for optical measurements (Khoram, et al., manuscript in preparation). Perovskite precursors, in a 1:1 ratio of CH_3NH_3Br and $PbBr_2$, were dissolved in either dimethylformamide (DMF) or dimethyl sulfoxide (DMSO). The solution was spin-coated into a thin wet film on O_2-plasma-cleaned silica substrates (Methods, Supporting Information). Pressing this film face down into PDMS heated to 150°C produced the crystals. The thicknesses of the crystals used for measurements ranged from 155 to 1907

nm, with edge lengths between 3 and 20 μm. Crystals with thicknesses above ~500 nm appeared orange in accord with their strong absorption of light above the band gap (Figure 1a), while thinner crystals exhibited brilliant, thickness-dependent colors because of interference between the light reflected between their top and bottom facets (Figure 1b). The PDMS stamping technique yielded extremely smooth surface facets, typically exhibiting root-mean-square (RMS) roughness below 5 nm (Figure 1c-d), which allow for accurate reflectance and transmittance measurements with minimal scattering. A few representative measurements in an integrating sphere confirmed the absence of scattering.

The micro-reflectance and transmittance measurements were performed in a home-built optical setup (Figure 2). To acquire each spectrum, single-wavelength measurements were taken at 5-nm intervals between 405 and 1100 nm by focusing a supercontinuum light source modulated by an acousto-optic-tunable filter (Fianium, P ~ 0.1-3 kW cm^{-2}, full-width-half-maximum 2-4 nm) onto the surface of the crystal. Three photodetectors measured the incident, reflected, and transmitted light at each wavelength (Methods, Supporting Information). The small lateral size of the crystals necessitated the use of an objective to focus the spot to approximately 1-2 μm. The numerical aperture of the objective (NA 0.42) was low enough, however, for the incident beam to be well described as a plane wave (Supporting Information, Figure S1 and S2). The spectra typically showed strong absorptance at wavelengths below the band edge, and clear interference fringes appeared at longer wavelengths (Figure 3). For thicker crystals, the absorptance at wavelengths shorter than the band edge is flat and limited only by reflectance, while thinner crystals display a clear excitonic peak before the band edge and more widely spaced interference fringes after it.

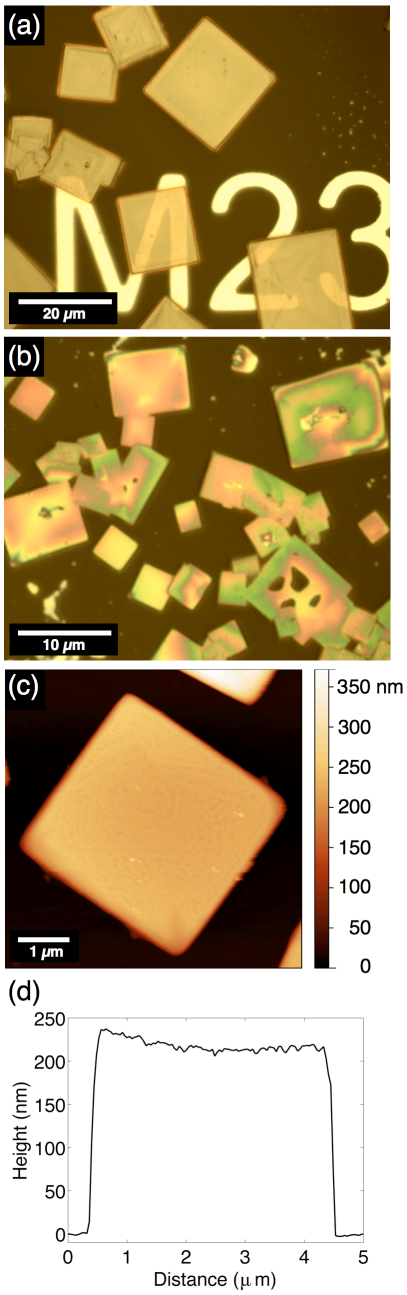

Figure 1. Flat and smooth crystals of $CH_3NH_3PbBr_3$. Brightfield optical images of thick (a) and thin (b) crystals deposited on fused silica substrates pre-patterned with TiO_x markers (M23) to locate the crystals. The brilliant colors of the thin (<500 nm) crystals arise from interference and depend on the thickness of the crystal. (c) Atomic force microscope (AFM) image of one microcrystal and (d) a line profile through its center. On

the surface of the crystal, the root-mean-square (rms) roughness is below 5 nm, and the slope of the surface is less than 1°.

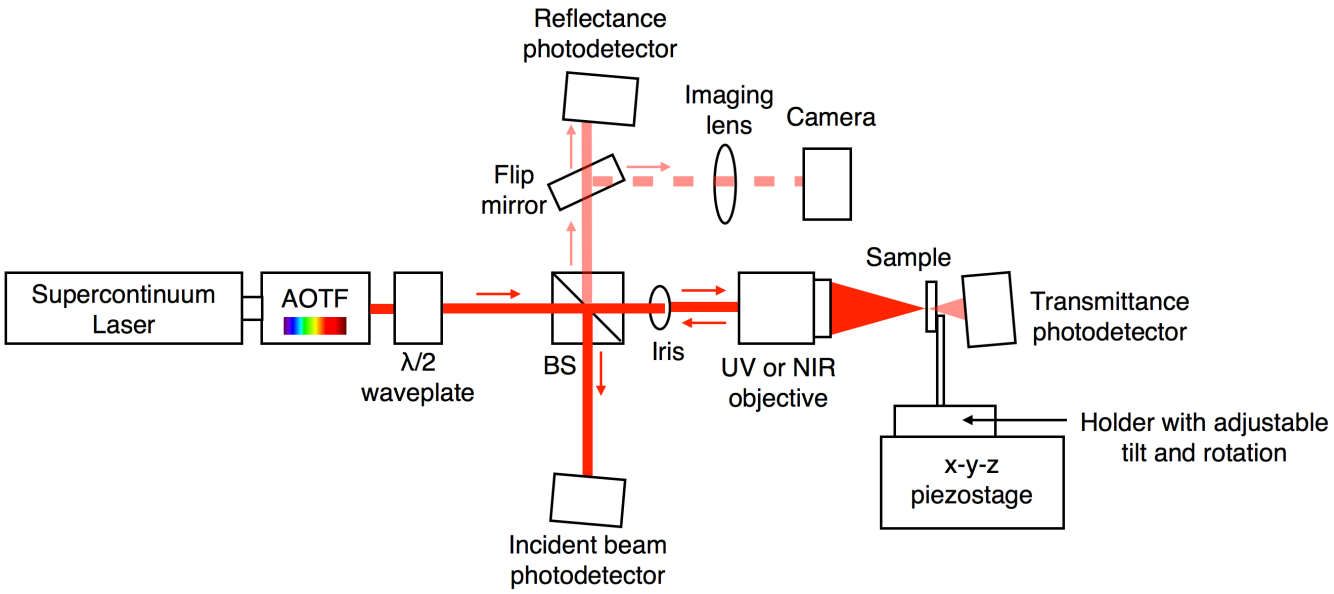

Figure 2. Schematic of the optical measurement setup. Light from a supercontinuum laser was filtered by an acousto-optic tunable filter (AOTF) and focused by an objective onto the sample, which was mounted on a piezostage. Three photodetectors measured the incident, transmitted, and reflected beams at each wavelength produced by scanning the AOTF. A half-wave plate was used to control the laser's polarization. A flip mirror, lens, and camera were used to image the sample to locate the crystals. Additional details of the setup and calibration procedures can be found in the Methods section of the Supporting Information.

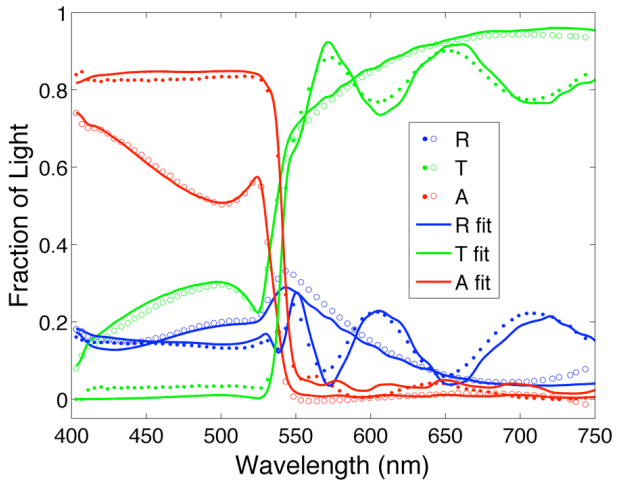

Figure 3. Optical spectra of two microcrystals in the visible region of the spectrum. Experimental reflectance (R), transmittance (T), and absorptance (A) of a thin, 180-nm crystal (open circles) and a thick, 815-nm crystal (filled circles). The plotted fits to the data points are calculated based on the extracted *n* and *k* values and model the crystal as a flat thin film on a non-absorbing fused silica substrate.

Because of thin-film interference, reflectance and transmittance are oscillatory functions, and multiple *n*-*k* pairs exist as solutions at each wavelength[18, 31] for each crystal (Supporting Information, Figure S3); consequently, without further assumptions and constraints on the thickness of the film,[16] determination of the unique optical constants from measurements at normal incidence on a film with a single thickness is not possible. Measuring crystals of multiple thicknesses solves this dilemma, however, because the spurious *n*-*k* pairs shift with thickness because of interference, while the true values of *n* and *k* appear as solutions common to all samples (Supporting Information, Figure S3). While one could directly invert the data from each crystal and look for the *n*-*k* solutions that do not change between crystals, experimental error complicates this approach. Because measurements are not exact, gaps in the solutions appear near the real *n*-*k* values

near interference extrema,[31] causing the real solution not to appear in a direct inversion (Supporting Information, Figure S3).

Instead, to extract optical constants from the measured spectra, a nonlinear regression was applied independently at each wavelength to both reflectance and transmittance data from all of the crystals. Each crystal was modeled as a flat thin film on a transparent substrate illuminated by a plane wave. Reflection from the back surface of the thick but non-infinite substrate (500 μm) was assumed to be incoherent. Measurements were performed only at normal incidence, and the thickness of each crystal was determined using atomic force microscopy (AFM). The regression was applied at each wavelength using both reflectance and transmittance data from all of the crystals. This regression searches for the *n*-*k* pair that minimizes the deviation of all the experimental spectra from the predicted spectra based on the *n*-*k* pair. The regression essentially allows one to guess the real solution and confirm that the spectra calculated from it reproduce the experimental data. Performing a regression at a specific wavelength across many crystals also reduces the error in the extracted *n* and *k* values, as compared to extracting them from a single thickness. Because of the oscillatory nature of reflectance and transmittance, the error in *n* and *k* calculated from a single thickness diverges near critical points in the solution, such as the interference extrema.[32] Crystals of different thicknesses display these maxima at different wavelengths, so by measuring many thicknesses, one can be sure that there will be a crystal at each wavelength from which to determine the *n* and *k* values with sufficiently low error. This benefit is reflected in the fact that the slope of the regression's objective function near the minimum *n* and *k* values increases steeply

with minor adjustments to *n* and *k*, indicating that the determined values are firmly in a local minimum (Supporting Information, Figure S4).

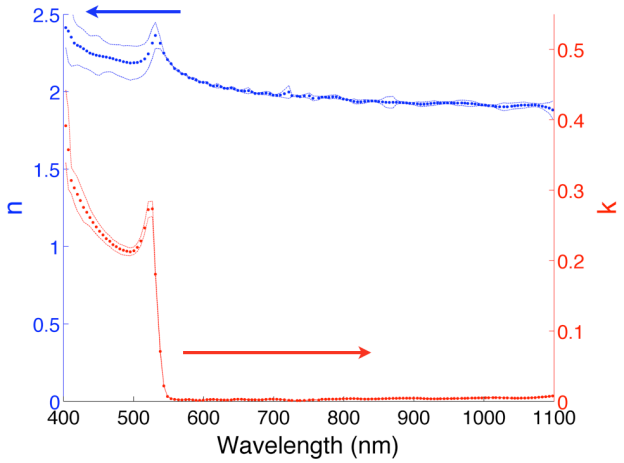

Figure 4. Extracted *n* and *k* values. At each wavelength, a non-linear regression was applied to the experimental reflectance and transmittance spectra of 22 crystals to obtain the *n* and *k* values that minimized the deviation between the calculated and experimental spectra. Solid points are the extracted final values, and the dotted lines indicate an estimate of the experimental error. Such error bounds, however, do not account for any systematic error in the measurements. The supporting information includes a text file of the plotted data.

These regressions at each wavelength produce the *n* and *k* values of $CH_3NH_3PbBr_3$ (Figure 4). Error in *n* and *k* at each wavelength caused by random error in the experimental measurements was estimated using del Pozo and Diaz's formula,[32] which derives the error in *n* and *k* for a single measurement from the experimental errors in reflectance, transmittance, and film thickness (*d*) and the derivatives of the reflectance and transmittance relations with respect to *n*, *k*, and *d*. Experimental error in reflectance and transmittance at each wavelength was estimated as the standard deviation of the

residuals at each wavelength (on average, 2.2 absolute percent in reflectance and 3.2 absolute percent in transmittance). Experimental error in the thickness measurements was estimated by performing a separate regression for each crystal fixing the *n* and *k* values to those determined collectively and allowing the thickness to vary to improve the match to the experimental spectra. These new thicknesses were then input back into the wavelength regressions to adjust the previously determined *n* and *k* values; the optical constants calculated from the optimized thicknesses were taken as the best values because further iteration produced negligible changes in thicknesses or in *n* and *k*. The standard deviation of these adjustments to the thicknesses (10.6 nm) was taken as the experimental error on the AFM measurements. From the error calculated for all of the crystals at each wavelength (Supporting Information, Figure S5), the minimum error at each wavelength point was plotted in Figure 3 because this error enforces the tightest bound on the extracted values of *n* and *k*. It should be emphasized, however, that these error bounds estimate only random and not systematic error in the measurements. For example, this distinction is clear in the non-zero value of *k* below the band edge, which appears because of experimental error in the calibration of the reflectance and transmittance measurements (Supporting Information, Figure S2).

These *n* and *k* values from rapidly crystallized microcrystals agree well with very recently published optical constants extracted via ellipsometry performed on macroscopic crystals (Figure 5a-b).[27] The 3% underestimation of *n* below the band edge in the thin crystals likely arises because no surface layer (oxide or roughness) was assumed, while such a layer (3.63 nm) was postulated in the ellipsometry model. It should also be noted that no model of the dielectric function was assumed or required during the extraction of

these *n* and *k* values from the microcrystals of varying thicknesses. Subsequently fitting a model of the dielectric function to the extracted optical constants confirms that the data is consistent with the Kramers-Kronig relations and can provide insight into the material's band structure,[30,33-34] such as estimates for the exciton binding energy and electronic band gap (Supporting Information, Figure S6).

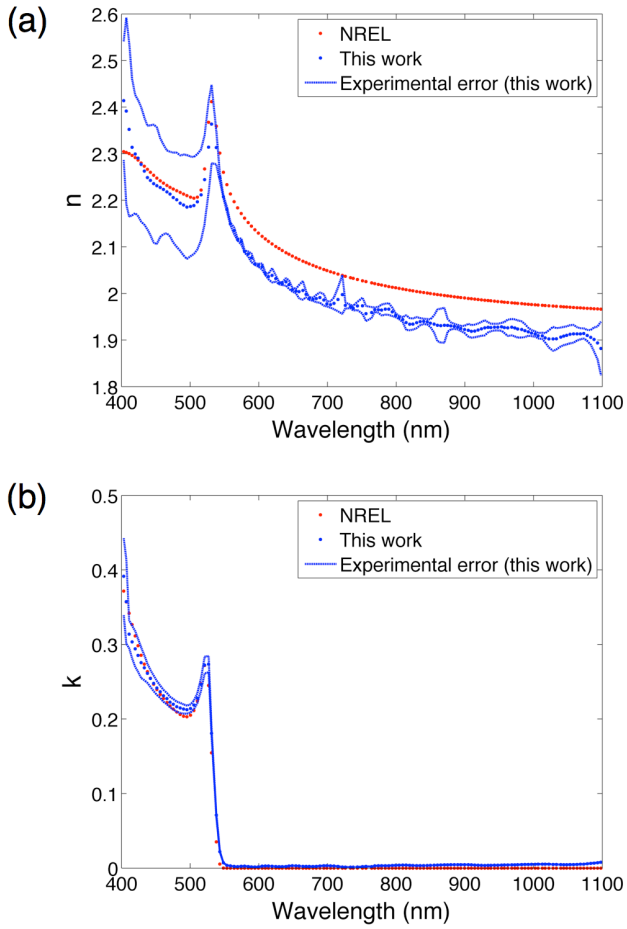

Figure 5. Comparison between optical constants extracted via ellipsometry and the values reported in this work. The ellipsometry data from the National Renewable Energy Laboratory (NREL) results from a fit with a multi-oscillator model.[27] The 3% deviation in *n* below the band edge likely arises from the fact that the model used for ellipsometry postulated a 3.63-nm surface layer.

In summary, a method for measuring *n* and *k* at the microscale in $CH_3NH_3PbBr_3$ has been presented, and its results agree with recent ellipsometry measurements on macroscopic $CH_3NH_3PbBr_3$ crystals produced by a solvothermal method.[27] Such microscale measurements of reflectance and transmittance can be applied to any material for which transmissive platelets of various thicknesses can be synthesized. This method is therefore appropriate for determining optical constants of solution- and vapor-processed micro- and nanoplatelets often found in the synthetic literature, and a related technique has been used to study two-dimensional (2D) materials.[28] Determination of optical constants is critical to the development of optoelectronic devices, including solar cells, photodetectors, LEDs, and lasers. In the case of $CH_3NH_3PbBr_3$, the clear excitonic peak at room temperature also suggests the possibility for future studies of exciton-polariton and exciton-plasmon effects in micro- and nanoscale optical devices. $CH_3NH_3PbBr_3$ is just one of the many hybrid and inorganic perovskites with such interesting optical properties. This method of measuring *n* and *k* at the microscale can be applied to other perovskites and can therefore be used to advance the design of optoelectronic devices made from these fascinating materials.

ASSOCIATED CONTENT

Supporting Information. Methods. FDTD simulations comparing reflectance from plane-wave and focused illumination and illumination at off-normal angles. Standard measurements of a 197-nm thick Si thin film and bulk silicon. The multiple *n*-*k* solutions that arise from direct inversion of the spectra from each crystal. AFM-measured and optimized thicknesses of the crystals. Minimization of the objective function for the

wavelength regression. Investigation of the error for measurements on each crystal. Modeling of the dielectric function based on critical points in the band structure. MAPbBr3.txt: a tab-delimited list of the wavelength, n, k, error in n, and error in k. This information is available free of charge via the Internet at http://pubs.acs.org.

AUTHOR INFORMATION

Notes

The authors declare no competing financial interests.

Corresponding Author

* Please address correspondence to Dr. Erik Garnett. Email: garnett@amolf.nl.

Telephone: +31 (0)20 754 7231.

ACKNOWLEDGMENT

The authors thank Sander Mann for helpful discussions on analyzing the data and Prof. Femius Koenderink for suggestions to improve the manuscript. This work is part of the research program of the Foundation for Fundamental Research on Matter (FOM), which is part of the Netherlands Organization for Scientific Research (NWO). The authors acknowledge financial support from the European Research Council under the European Union's Seventh Framework Programme (FP/2007-2013)/ERC Grant Agreement no. 337328, "NanoEnabledPV," and from an industrial partnership between Philips and FOM.

REFERENCES

1. Green, M. A.; Ho-Baillie, A.; Snaith, H. J. The Emergence of Perovskite Solar Cells. *Nature Photon*. **2014**, *8*, 506-514.

2. Tan, Z. K., et al. Bright Light-Emitting Diodes Based on Organometal Halide Perovskite. *Nature Nanotech*. **2014**, *9*, 687-92.

3. Sadhanala, A., et al. Blue-Green Color Tunable Solution Processable Organolead Chloride-Bromide Mixed Halide Perovskites for Optoelectronic Applications. *Nano Lett*. **2015**, *15*, 6095-101.

4. Deschler, F., et al. High Photoluminescence Efficiency and Optically Pumped Lasing in Solution-Processed Mixed Halide Perovskite Semiconductors. *J. Phys. Chem. Lett*. **2014**, *5*, 1421-6.

5. Xing, G.; Mathews, N.; Lim, S. S.; Yantara, N.; Liu, X.; Sabba, D.; Gratzel, M.; Mhaisalkar, S.; Sum, T. C. Low-Temperature Solution-Processed Wavelength-Tunable Perovskites for Lasing. *Nature Mater*. **2014**, *13*, 476-80.

6. Dou, L.; Yang, Y. M.; You, J.; Hong, Z.; Chang, W. H.; Li, G.; Yang, Y. Solution-Processed Hybrid Perovskite Photodetectors with High Detectivity. *Nat. Commun*. **2014**, *5*, 5404.

7. Fang, Y.; Dong, Q.; Shao, Y.; Yuan, Y.; Huang, J. Highly Narrowband Perovskite Single-Crystal Photodetectors Enabled by Surface-Charge Recombination. *Nature Photon*. **2015**, *9*, 679-686.

8. Lin, Q.; Armin, A.; Burn, P. L.; Meredith, P. Filterless Narrowband Visible Photodetectors. *Nature Photon*. **2015**, *9*, 687-694.

9. Sutherland, B. R.; Hoogland, S.; Adachi, M. M.; Wong, C. T. O.; Sargent, E. Conformal Organohalide Perovskites Enable Lasing on Spherical Resonators. *ACS Nano* **2014**, *8*, 10947-10952.

10. Zhang, Q.; Ha, S. T.; Liu, X.; Sum, T. C.; Xiong, Q. Room-Temperature near-Infrared High-Q Perovskite Whispering-Gallery Planar Nanolasers. *Nano Lett*. **2014**, *14*, 5995-6001.

11. Xing, J.; Liu, X. F.; Zhang, Q.; Ha, S. T.; Yuan, Y. W.; Shen, C.; Sum, T. C.; Xiong, Q. Vapor Phase Synthesis of Organometal Halide Perovskite Nanowires for Tunable Room-Temperature Nanolasers. *Nano Lett*. **2015**, *15*, 4571-7.

12. Zhu, H.; Fu, Y.; Meng, F.; Wu, X.; Gong, Z.; Ding, Q.; Gustafsson, M. V.; Trinh, M. T.; Jin, S.; Zhu, X. Y. Lead Halide Perovskite Nanowire Lasers with Low Lasing Thresholds and High Quality Factors. *Nature Mater*. **2015**, *14*, 636-42.

13. Wong, A. B.; Lai, M.; Eaton, S. W.; Yu, Y.; Lin, E.; Dou, L.; Fu, A.; Yang, P. Growth and Anion Exchange Conversion of Ch3nh3pbx3 Nanorod Arrays for Light-Emitting Diodes. *Nano Lett*. **2015**, *15*, 5519-24.

14. Brittman, S.; Adhyaksa, G. W.; Garnett, E. C. The Expanding World of Hybrid Perovskites: Materials Properties and Emerging Applications. *MRS Commun*. **2015**, *5*, 7-26.

15. Poelman, D.; Smet, P. F. Methods for the Determination of the Optical Constants of Thin Films from Single Transmission Measurements: A Critical Review. *J. Appl. Phys. D: Appl. Phys.* **2003**, *36*, 1850-1857.

16. Swanepoel, R. Determination of the Thickness and Optical Constants of Amorphous Silicon. *J. Phys. E: Sci. Instrum.* **1983**, *16*, 1214-1222.

17. Thompkins, H. G.; Irene, E. A., eds. *Handbook of Ellipsometry*; William Andrew: Norwich, NY, **2005**.

18. Palik, E. D., ed. *Handbook of Optical Constants of Solids, I and II*; Academic Press: San Diego, **1998**.

19. Djurišić, A. B.; Chan, Y.; Li, E. H. Progress in the Room-Temperature Optical Functions of Semiconductors. *Mat. Sci. Eng. R* **2002**, *38*, 237-293.

20. Stagg, B. J.; Charalampopoulos, T. T. Surface-Roughness Effects on the Determination of Optical Properties of Materials by the Reflection Method. *Appl. Opt.* **1991**, *30*, 4113-4118.

21. Jellison, G. E.; McCamy, J. W. Sample Depolarization Effects from Thin Films of ZnS on Gaas as Measured by Spectroscopic Ellipsometry. *Appl. Phys. Lett.* **1992**, *61*, 512.

22. Laaziz, Y.; Bennouna, A. On Some Important Care to Take When Making Spectrophotometric Measurements on Semiconductor Thin Films. *Thin Solid Films* **1995**, *277*, 155-161.

23. Loper, P.; Stuckelberger, M.; Niesen, B.; Werner, J.; Filipic, M.; Moon, S. J.; Yum, J. H.; Topic, M.; De Wolf, S.; Ballif, C. Complex Refractive Index Spectra of Ch3nh3pbi3 Perovskite Thin Films Determined by Spectroscopic Ellipsometry and Spectrophotometry. *J. Phys. Chem. Lett.* **2015**, *6*, 66-71.

24. Lin, Q.; Armin, A.; Nagiri, R. C. R.; Burn, P. L.; Meredith, P. Electro-Optics of Perovskite Solar Cells. *Nature Photon.* **2014**, *9*, 106-112.

25. Grancini, G.; Srimath Kandada, A. R.; Frost, J. M.; Barker, A. J.; De Bastiani, M.; Gandini, M.; Marras, S.; Lanzani, G.; Walsh, A.; Petrozza, A. Role of Microstructure in the Electron–Hole Interaction of Hybrid Lead Halide Perovskites. *Nature Photon.* **2015**.

26. Choi, J. J.; Yang, X.; Norman, Z. M.; Billinge, S. J.; Owen, J. S. Structure of Methylammonium Lead Iodide within Mesoporous Titanium Dioxide: Active Material in High-Performance Perovskite Solar Cells. *Nano Lett.* **2014**, *14*, 127-33.

27. Park, J.-S.; Choi, S.; Yan, Y.; Yang, Y.; Luther, J. M.; Wei, S.-H.; Parilla, P.; Zhu, K. Electronic Structure and Optical Properties of α-$CH_3NH_3PbBr_3$ perovskite Single Crystal. *J. Phys. Chem. Lett.* **2015**, 4304-4308.

28. Li, Y.; Chernikov, A.; Zhang, X.; Rigosi, A.; Hill, H. M.; van der Zande, A. M.; Chenet, D. A.; Shih, E.-M.; Hone, J.; Heinz, T. F. Measurement of the Optical Dielectric Function of Monolayer Transition-Metal Dichalcogenides: MoS_2, $MoSe_2$, WS_2, and WSe_2. *Phys. Rev. B* **2014**, *90,* 205422.

29. Stokowski, S. E. Measuring Refractive Indices of Films on Semiconductors by Micro-Reflectometry. *Proc. SPIE 1261, Integrated Circuit Metrology, Inspection, and Process Control IV* **1990**, 253-263.

30. Djurišić, A. B.; Chan, Y.; Li, E. H. The Model Dielectric Function: Application to GaSb and InP. *Semicond. Sci. Technol.* **2001**, *16*, 902-908.

31. Stichauer, L.; Gavoille, G. Effect of Experimental Errors on the Determination of Optical Constants of Thin Films. *Phys. Stat. Sol. A* **1993**, *135*, K41-K44.

32. del Pozo, J. M.; Díaz, L. Method for the Determination of Optical Constants of Thin Films: Dependence on Experimental Uncertainties. *Appl. Opt.* **1992**, *31*, 4474-4481.

33. Cardona, M.; Yu, P. *Fundamentals of Semiconductors: Physics and Materials Properties, 4th Ed.*; Springer: Berlin, **2010**.

34. Yang, Y.; Yan, Y.; Yang, M.; Choi, S.; Zhu, K.; Luther, J. M.; Beard, M. C. Low Surface Recombination Velocity in Solution-Grown $CH_3NH_3PbBr_3$ Perovskite Single Crystal. *Nat. Commun.* **2015**, *6*, 7961.

TOC graphic

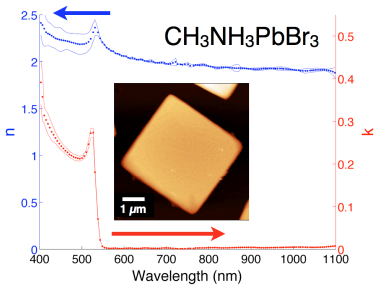
CH3NH3PbBr3
n
k
1 μm
Wavelength (nm)
400
500
600
700
800
900
1000
1100
0
0.5
1
1.5
2
2.5
0.1
0.2
0.3
0.4
0.5